ELSEVIER

Journal of Molecular Catalysis A: Chemical 160 (2000) 409–427

JOURNAL OF MOLECULAR CATALYSIS A: CHEMICAL

www.elsevier.com/locate/molcata

Molecular simulation on hydrodesulfurization of thiophenic compounds over MoS_2 using ZINDO

Xiaoliang Ma *, Harold H. Schobert

The Energy Institute, The Pennsylvania State University, University Park, PA 16802, USA

Received 15 February 2000; accepted 11 May 2000

Abstract

In order to develop a fundamental understanding of the HDS mechanism of thiophenic compounds over molybdenum disulfide (MoS_2), a molecular simulation of the hydrodesulfurization (HDS) of thiophenic compounds over MoS_2 has been performed using Zerner's Intermediate Neglect of Differential Overlap (ZINDO) program. On the basis of the calculated edge structure, stoichiometry of MoS_2, shape of the crystal, and the size corresponding to real MoS_2 particles, a single-slab cluster, $Mo_{27}S_{54}$, has been proposed for modeling the highly dispersed MoS_2. The proposed cluster is a regular hexagon with $(\bar{1}010)$ and $(30\bar{3}0)$ edge planes only. According to the calculated electronic properties of the surface, the coordinately unsaturated Mo_{IV} in the $(30\bar{3}0)$ plane is expected to be the active site for hydrogenation of thiophenic and aromatic compounds. The most stable adsorption configuration of thiophene on the Mo_{IV} is a flat adsorption configuration via the η^5-bound coordination, whereas the most stable adsorption configuration of tetrahydrothiophene (THT) on the Mo_{IV} is a tilted adsorption configuration via the S-bound coordination. HDS mechanism of thiophene through the hydrogenation pathway over the $(30\bar{3}0)$ plane of MoS_2 is discussed according to quantum chemical insights in combination with experimental results from the literature.

Keywords: Hydrodesulfurization; Thiophene; Molybdenum disulfide; ZINDO calculation; Heterogeneous catalysis

1. Introduction

Molybdenum sulfide species have been used commercially as hydrotreating catalysts for more than 70 years. A useful survey of the early literature, including the patent literature, was provided by Killeffer and Linz [1]. One of the important reactions involved in the hydrotreating processes is hydrodesulfurization (HDS), in which sulfur compounds, especially the thiophenic compounds, in feed stocks are removed by hydrogenation or hydrogenolysis in the presence of molybdenum sulfide catalysts. A fundamental understanding of the HDS active sites and the mechanism of such catalysts is essential for developing efficient catalysts and processes for so-called deep HDS, in which the sulfur content in feed is required to be less than 0.05 wt.%. Consequently, a large number of experimental studies have been devoted to finding the active sites on the catalyst surface and to exploring the HDS mechanism of thiophenic compounds on them. The major approaches can be grouped into three general areas: (1) kinetics

* Corresponding author. Tel.: +1-814-863-8744; fax: +1-814-863-8892.

E-mail address: mxx2@psu.edu (X. Ma).

1381-1169/00/$ - see front matter
PII: S1381-1169(00)00278-8

and poisoning; (2) characterization of catalyst surface structure using advanced spectroscopic techniques; and (3) coordination chemistry of organometallic complexes.

The kinetics and poisoning investigations have indicated that HDS of thiophenic compounds proceeds through two pathways, a hydrogenation pathway (hydrogenation followed by hydrogenolysis) and a hydrogenolysis pathway (direct elimination of S atom) [2–8]. Hydrogenation and hydrogenolysis probably occur at different active sites. H_2S was found to be one of the main inhibitors of the hydrogenolysis pathway [9–15], while polyaromatic compounds were found to be the main inhibitors of the hydrogenation pathway [9,15–17]. Some excellent reviews of this aspect of HDS research are available in the literature [18,19]. With respect to the characterization of catalyst surface structure, various models for the active site structures have been proposed on the basis of surface characterization using X-ray diffraction (XRD), scanning electron microscopy (SEM), transmission electron microscopy (TEM), and Mössbauer emission spectroscopy (MES). Especially within the past several years, the detailed structural elucidation of molybdenum sulfide species has been achieved through the use of high-energy techniques such as X-ray photoelectron spectroscopy (XPS), extended X-ray absorption fine structure (EXAFS) spectroscopy, and X-ray absorption near-edge structure (XANES) spectroscopy. It was found that there are coordinatively unsaturated Mo atoms on the surface. Whitehurst et al. [19] and Topsøe et al. [20] have published excellent reviews of this aspect. The coordination chemistry investigations have found that there are S-, η^2-, η^4-, η^5-, η^4-, S-μ_2-, and η^4-, S-μ_3-bound models in organometallic complexes for thiophene coordination with transition metal complexes [21–25]. These models indicate likely adsorption configurations of thiophene on the active sites of the catalyst surface. Recently, Jones et al. [26] and Bianchini and Meli [27] respectively reviewed hydrogenation, hydrogenolysis, and desulfurization of thiophenes by soluble metal complexes, which provides an important insight into the HDS mechanism.

Since it is still difficult experimentally to characterize the chemical properties of the catalyst surface and the adsorbates, especially at the actual reaction conditions, many attempts at the computational simulation of thiophene HDS over molybdenum sulfide catalysts have been made on the basis of various cluster models. Many cluster models, MoS_6 [28], a-Mo_3S_6 [29], b-Mo_3S_6 [30,31], Mo_2S_{14} [32], a-Mo_3S_{14} [30,32], b-Mo_3S_{14} [32,33], Mo_7S_{14} [33], Mo_4S_{12} [33], Mo_5S_{10} [30], Mo_5S_{12} [34], Mo_6S_{14} [28], $Mo_{19}S_{38}$ [32,35], etc. have been proposed to mimic molybdenum disulfide (MoS_2) surface or particles [28–37]. However, there are yet some problems in these models: (1) The clusters are not stoichiometric or electroneutral; (2) The clusters are too small to mimic the real MoS_2 catalyst surface; (3) The surface structure in the clusters is unlikely, although not impossible; and/or (4) Some studies use empirical approximation or the Extended Hückel approximation that give a relatively lower accuracy. Such problems may give rise to inaccurate or even incorrect information about MoS_2 surface. In order to overcome these problems, Byskov et al. [38] used an one-dimensional periodic unit cell (Mo_4S_8) as a model of MoS_2 surface and calculated it by using self-consistent density functional theory (DFT). They found that reconstructions occur at the MoS_2 edges. By comparison of the sulfur binding energy ($\Delta E(S_{III}) > \Delta E(S_I) > \Delta E(S_{II})$), the subscript is the coordinative number of the S atom) they concluded that vacancies created at the S edges (S_{II} position) apparently provide the most easily accessible active sites. Tan and Harris [39] extended the Fenske–Hall molecular orbital technique to two- and three-dimensional periodic unit cells to study the bulk and surface electronic structure of MoS_2. By comparison of Mo–S overlap populations (Mo–S_I > Mo–S_{II} > Mo–S_{III}), they concluded that removal of terminal S_I atoms to form coordinatively unsaturated Mo sites may

be more difficult than removal of either bridging S (S_{II}) or tribonding S (S_{III}). Raybaus et al. [40,41] used a three-dimensional periodic unit cell ($Mo_{24}S_{48}$) as a model of MoS_2 surface, and calculated it by using ab initio local-density-function molecular dynamics. They found that the terminated surfaces ($\bar{1}010$, $30\bar{3}0$) remain stable in vacuum up to temperature of 700 K, with only modest relaxation of the surface atoms. By calculation, they gave an adsorption configuration of thiophene through a bridge–η^5 bonding to two Mo_{IV} atoms, with the molecular ring approximately parallel to the surface ($30\bar{3}0$). This adsorption configuration is different from the conclusion that the adsorption configuration perpendicular to the active surface (Mo_{IV}) is favored, by Pis Diez and Jubert [33] using the Extended Hückel theory. This adsorption configuration is also somewhat different from that reported in our previous study [42], though both are the flat adsorption configurations. As mentioned above, the results from different investigators are distinct from each other, making it difficult to draw meaningful conclusions about the active sites and adsorption configuration of thiophenic compounds on the active sites.

A significant advantage of using the periodic unit cell as a model to study the MoS_2 surface is that it decreases the computational cost for calculating a large MoS_2 cluster. However, we need to keep in mind that for the highly dispersed supported MoS_2 catalysts, the predominant sizes of MoS_2 particles are within 10–30 Å [35,43,44]. This indicates that there should be only two, three or four Mo atoms (or S pairs) on a corresponding edge plane, which will be discussed in detail later. The electron properties of each Mo atom (or S pairs) at different positions of the edge planes should be different due to a corner effect. Therefore, using a MoS_2 cluster with the size corresponding to real MoS_2 catalyst particles as a model instead of the periodic unit cell may be more reasonable.

In order to simulate the surface structure of a highly dispersed MoS_2 particle, it is very important to build up a reasonable MoS_2 cluster model with correct stoichiometry and electroneutrality, stable peripheral structure, and a size corresponding to the real MoS_2 particles. In our previous work based on a semiempirical calculation [45], we proposed regular hexagonal clusters, $Mo_{12}S_{24}$ and $Mo_{27}S_{54}$, for modeling a single slab of MoS_2, the edges of which consist of the ($\bar{1}010$) and ($30\bar{3}0$) edge planes only. These models are stoichiometric and electroneutral clusters without any saturating H atom and without charge compensation. Very recently, Faye et al. [46] employed the $M_{12}S_{24}$ cluster in their density functional approach of γ-alumina-supported MoS_2.

In order to develop a fundamental understanding of the HDS mechanism of thiophenic compounds over MoS_2, we performed a systematic molecular simulation using Zerner's Intermediate Neglect of Differential Overlap (ZINDO) program in this study. We attempted to perfect the previously proposed MoS_2 clusters, to find the active sites on the surface of MoS_2 clusters, and, moreover, to examine how such active sites interact with sulfur species. Adsorption configurations of sulfur species on the active sites and their implication in the HDS mechanism will be discussed according to quantum chemical insights.

2. Modeling and computational method

Single-slab MoS_2 clusters were used in this study. The crystal structure sizes of MoS_2 used in this study are from X-ray data in the literature. It needs to be mentioned that the crystal structure sizes from different references are somewhat different. In our previous study [42,45], we used the data from Wyckoff [47] and from Joffer et al. [48]. In the present study, we employed the data (space group: $P3(3)/MMC$, $a = 3.153$ Å, $c = 12.300$ Å) from a new version (1991) of the handbook edited by Daams et al. [49] as the latter may be more reliable. The Mo–S coordination distance in bulk MoS_2 was used for the edge structure of the clusters,

as no significant difference of coordination distance has been observed experimentally between the edge and bulk of MoS_2 [50,51]. The crystal structure of the single-slab MoS_2 consists of "sandwiches" in which one planar layer of molybdenum atoms is interspersed between two layers of sulfur atoms as shown in Fig. 1. Within the single slab, each S atom in basal plane is equidistant from three Mo atoms, and each Mo atom is surrounded by six equidistant S atoms at the corners of a trigonal prism with altitude and edge dimension of 3.173 and 3.153 Å, respectively. The Mo–S bond length is 2.415 Å.

All quantum chemical calculations in this study, except where specifically mentioned, were performed by ZINDO in the Computer Aided Chemistry (CAChe) using atomic units (a.u.). ZINDO is a series of molecular electronic programs that have been developed over the last 20 years both at the University of Guelph and at the University of Florida [52–59]. Due to the approximate nature of the Hamiltonians in ZINDO, the time required to run a ZINDO calculation in only a fraction of that required by first-principles programs. ZINDO uses a well-validated technology as supported by a large number of scientific publications [60]. Geometry of thiophene, dibenzothiophene (DBT), H_2S, tetrahydrothiophene (THT) and naphthalene was optimized using theoretical Intermediate Neglect of Differential Overlap (INDO/1) parameters in ZINDO, as the theoretical INDO/1 parameters give better geometry than the spectroscopic INDO/1 parameters [53,54,57,59]. The optimized sulfur compounds and naphtha-

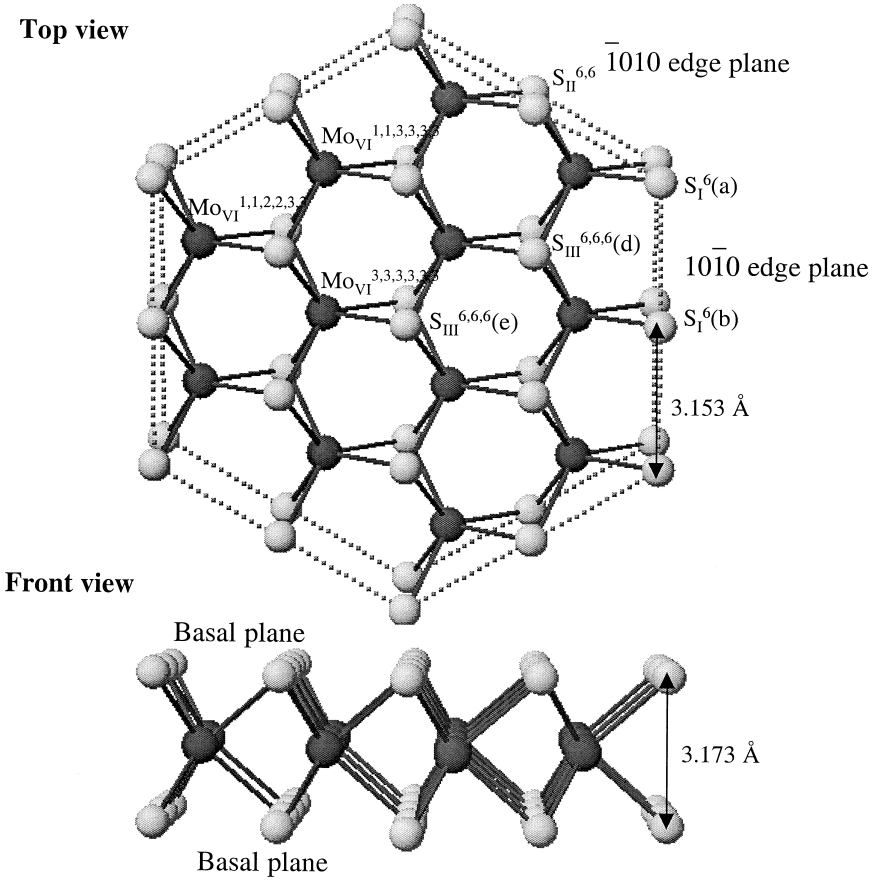

Fig. 1. Single slab of $Mo_{12}S_{38}$ cluster.

lene were located at different assigned positions at the cluster to form various adsorption configurations. The clusters and adsorbate–cluster systems were calculated without further geometric optimization. Electronic properties and total energies (the core repulsion energies) of the compounds, clusters and adsorbate–cluster systems were calculated using the spectroscopic INDO/1 parameters as use of the spectroscopic INDO/1 parameters results in better electron densities, charges, and bond indexes [55,56,58]. For Mo atom, the theoretical INDO/1 parameters were used since the spectroscopic INDO/1 parameters for Mo atom are unavailable. The formal charge values for each atom in the compounds, clusters, and adsorbate–clusters were calculated by the population study in the Zero Differential Overlap (ZDO) basis. Electrostatic potentials of the sulfur compounds and the clusters were calculated using the multiple expansion.

In order to compare the calculated results conveniently, a pseudo-adsorption heat was used in this study, which is defined as follows:

$$\underset{E_a}{\text{adsorbate}} + \underset{E_c}{\text{cluster}} \rightarrow \underset{E_{a-c}}{\text{adsorbate–cluster}}$$

$$\text{Pseudo-adsorption heat}\,(\Delta H) = E_{a-c} - (E_a + E_c)$$

where, E_a, E_c, and E_{a-c} are the energy corresponding to the adsorbate, cluster, and adsorbate–cluster, respectively. Since the geometry of the molecules adsorbed on surface of the cluster was not optimized in the calculations, the absolute values of the calculated ΔH may be inaccurate. However, we believe that the relative ΔH values should make sense in a comparison of the stability of various adsorption configurations.

The geometries of thiophene and THT for the electrostatic potential calculation were optimized by the Molecular Orbital Package-Parametric Method 3 (MOPAC-PM3) method [61,62] since the MOPAC-PM3 method gives a higher accuracy than the ZINDO method.

3. Results and discussion

3.1. MoS_2 cluster model

The crystal structure of MoS_2 has been known for a long time [63], but the peripheral structure of the MoS_2 crystal, even for a single slab, is still unclear. There are a large number of possible peripheral configurations from the point of view of morphology [64]. However, MoS_2 is quite unreactive chemically, even at elevated temperature. As a catalyst for hydrotreatment, its catalytic activity is very stable at temperatures as high as 400°C. Hence, we believe that the most stable peripheral structure should be the most probable one.

3.1.1. Peripheral structure of a MoS_2 single slab

In order to seek a stable peripheral structure of MoS_2, we first examine a single slab of regular hexagonal $Mo_{12}S_{38}$ cluster, as shown in Fig. 1. The peripheral edges of this cluster consist of $(\bar{1}010)$ and $(10\bar{1}0)$ planes only. Each Mo atom in the cluster is coordinated to six S atoms without any coordinatively unsaturated Mo atom. The S atoms in the cluster can be classified into three groups according to their coordinative environment: terminal S atoms, bridged S atoms, and tribound S atoms, which are symbolized by S_I^6, $S_{II}^{6,6}$, and $S_{III}^{6,6,6}$, respectively. The superscript is the coordinative number of each Mo atom neighboring to the S atom. The S/Mo atomic ratio in the cluster is 3.17, much higher than the stoichiometry of MoS_2.

Many investigators have demonstrated that there are coordinatively unsaturated sites (CUS) (e.g. sulfur vacancies) on the MoS_2 surface on the basis of the spectroscopic characterization [50,51,65,66], poisoning studies [20] and chemisorption of probe molecules [20]. On the other hand, according to chemical analysis the S/Mo stoichiometry in MoS_2 catalysts is preserved with a good accuracy [67–70]. Qian et al. [71] reported that the S/Mo stoichiometry in

Table 1
Formal charge of the atoms in $Mo_{12}S_{38}$ cluster

Atom	Number	Average charge (a.u.)
S_I^6	18	−0.440
$S_{II}^{6,6}$	6	−0.659
$S_{III}^{6,6,6}$	14	−0.667
$Mo_{VI}^{1,1,2,2,3,3}$	6	1.915
$Mo_{VI}^{1,1,3,3,3,3}$	3	1.756
$Mo_{VI}^{3,3,3,3,3,3}$	3	1.484

a sulfided Mo/Al_2O_3 catalyst is 1.92 at the real HDS conditions. Recently, Calais et al. [72] found that for the highly dispersed unsupported MoS_2, the stoichiometry of S/Mo is around 2.0 when the temperature increased to 200°C during the TPR (temperature-programmed reduction) experiments. To form CUS at the edges of the $Mo_{12}S_{38}$ cluster and to retain the MoS_2 stoichiometry in the $Mo_{12}S_{38}$ cluster, it is evident that excess or non-stoichiometric sulfur atoms in the $Mo_{12}S_{38}$ cluster have to be removed. Thus, our question becomes one of determining which kinds of S atoms can be reasonably removed from the cluster in view of the energetics and electronic properties of the surface.

The calculations of charge distribution and bond index for the $Mo_{12}S_{38}$ cluster were performed. The results are given in Tables 1 and 2, respectively. According to the calculated results, sulfur atoms in the cluster show a negative charge, while Mo atoms show a positive charge. The charge value of each S atom is primarily dependent on its coordinative environment. It was found that sulfur atoms with the same coordinative environment show a similar charge value, the average values being −0.440, −0.659, and −0.667 a.u. for S_I^6, $S_{II}^{6,6}$, and $S_{III}^{6,6,6}$, respectively.

The Wybery bond index that coincides closely with the bond order was calculated for the cluster and the results are listed in Table 2. It was found that all bond indexes between neighboring S and Mo atoms are higher than 0.79, while the bond indexes between two neighboring S atoms and two neighboring Mo atoms are low, being less than 0.10 and 0.31, respectively. The results clearly imply that there is a strong interaction between neighboring S and Mo atoms, and the atoms in MoS_2 lattice are held together dominantly through such bonding.

The terminal S atoms (S_I^6) in the $(10\bar{1}0)$ edge planes are bonded to only one Mo atom with an average S_I^6–M_{VI} bond index of 1.041. The bridged S atoms ($S_{II}^{6,6}$) in the $(\bar{1}010)$ edge planes are bonded to two neighboring Mo atoms with a $S_{II}^{6,6}$–$Mo_{VI}^{1,1,2,2,3,3}$ bond index of 1.010. The tribound S atoms ($S_{III}^{6,6,6}$) in the basal planes are bonded to three neighboring Mo atoms simultaneously with a $S_{III}^{6,6,6}$–$Mo_{VI}^{3,3,3,3,3,3}$ bond index of 0.823. The sum of three bond indexes for the $S_{III}^{6,6,6}$ atoms is greater than 2.460, indicating they have the strongest interaction with the MoS_2 bulk. By comparing the bond indexes, it is clear that in all of the S atoms in the cluster the S_I atoms in the $(10\bar{1}0)$ edge planes are the easiest to be removed from the cluster to form CUS, while the sulfur atoms in the basal plane are the most stable. The results are in contraction with the conclusion by Tan and Harris [39], although our calculated Mo–S bond orders are roughly consistent with their calculated Mo–S

Table 2
Bond indexes in $Mo_{12}S_{38}$ cluster

S–Mo	Bond index	Mo–Mo	Bond index	S–S	Bond index
S_I^6(a)–$Mo_{VI}^{1,1,2,2,3,3}$	1.069	$Mo_{VI}^{1,1,2,2,3,3}$–$Mo_{VI}^{1,1,3,3,3,3}$	0.191	S–S	< 0.100
S_I^6(b)–$Mo_{VI}^{1,1,3,3,3,3}$	0.984	$Mo_{VI}^{1,1,2,2,3,3}$–$Mo_{VI}^{1,1,2,2,3,3}$	0.271		
$S_{II}^{6,6}$(c)–$Mo_{VI}^{1,1,2,2,3,3}$	1.010	$Mo_{VI}^{1,1,2,2,3,3}$–$Mo_{VI}^{3,3,3,3,3,3}$	0.283		
$S_{III}^{6,6,6}$(d)–$Mo_{VI}^{1,1,2,2,3,3}$	0.831	$Mo_{VI}^{1,1,3,3,3,3}$–$Mo_{VI}^{3,3,3,3,3,3}$	0.277		
$S_{III}^{6,6,6}$(d)–$Mo_{VI}^{1,1,3,3,3,3}$	0.792	$Mo_{VI}^{3,3,3,3,3,3}$–$Mo_{VI}^{3,3,3,3,3,3}$	0.307		
$S_{III}^{6,6,6}$(d)–$Mo_{VI}^{3,3,3,3,3,3}$	0.830				
$S_{III}^{6,6,6}$(e)–$Mo_{VI}^{3,3,3,3,3,3}$	0.823				

overlap populations. Probably, they did not take account of the fact that the S_{III} atoms are bonded to three neighboring Mo atoms simultaneously.

In addition, the calculation of the total energy for the clusters with a S vacancy at different positions was also performed. The total energies of the clusters with a S vacancy at S_I^6(a), $S_{II}^{6,6}$, $S_{III}^{6,6,6}$(d) and $S_{III}^{6,6,6}$(e) (see Fig. 1) are −524.00, −523.41, −522.52, and −522.14 (a.u.), respectively, indicating the S_I^6(a) vacancy is the most stable in the four cases. In other words, the facilitation for removing sulfur from the MoS_2 surface is in the order of $S_I > S_{II} > S_{III}$, which further supports the point that S vacancies should be formed more readily in the $(10\bar{1}0)$ planes than in others. This result is different from that ($S_{II} > S_I > S_{III}$) obtained by Byskov et al. [38]. The reasons for this discrepancy probably are: (1) as mentioned by Byskov et al., the relatively narrow model was used in their calculation and (2) in our model, the surface atoms were not relaxed. It is generally believed that the activity of the sulfur atoms in the surface will be inversely proportional to their coordinative saturation. From this view, our results seem to be more reasonable. The result that the tribound S_{III} atoms are difficult to be removed than the S_{II} and S_I atoms from the MoS_2 surface is in good agreement with the work by Byskov et al. [38] and the surface science experiments [73].

3.1.2. Stoichiometry, shape, and particle size of MoS_2

If CUS on the $(10\bar{1}0)$ edge planes and the stoichiometry of MoS_2 were the only consideration we could still draw up many clusters, as shown in Fig. 2. All these clusters, including the linear ($Mo_{2n+1}S_{4n+2}$), rhomboidal ($Mo_{3n+2}S_{6n+4}$) and regular hexagonal ($Mo_{3n^2}S_{6n^2}$) clusters (n is the number of Mo_{IV}

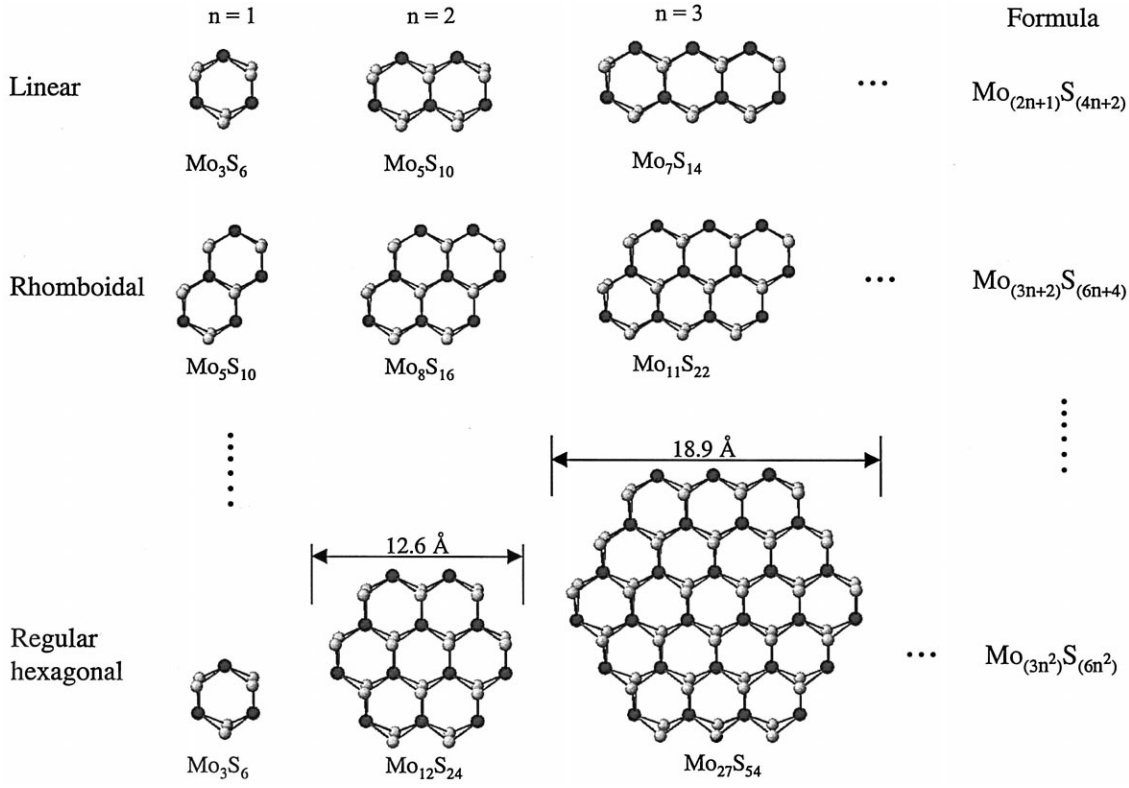

Fig. 2. Stoichiometric MoS_2 clusters with CUS in the $(30\bar{3}0)$ planes only; n: the number of Mo_{IV} in the top $(30\bar{3}0)$ edge plane.

atoms in the top $(30\bar{3}0)$ edge plane, see Fig. 2), have the stoichiometry of 2, and their peripheral edges consist of $(\bar{1}010)$ and $(30\bar{3}0)$ edge planes only. However, from natural mineral crystals of MoS_2 [63,74] and from the SEM of MoS_2 microcrystals [75], it was found that the angle included between two edge planes is always 120° regardless of stacking numbers. Only regular hexagonal clusters $(Mo_{3n^2}S_{6n^2})$ in Fig. 2 are consistent with this requirement. In order to demonstrate theoretically that the regular hexagonal clusters are the most stable ones, the total energies of various clusters as displayed in Fig. 2 were calculated. The unit energy per MoS_2 atomic group (the total energy divided by the total numbers of MoS_2 atomic group in the cluster) for each cluster as a function of the number of the MoS_2 atomic groups is shown in Fig. 3. It is clear that for the comparable number of the MoS_2 atomic groups the regular hexagonal clusters have the lowest unit energy, demonstrating that the regular hexagonal clusters is the most stable form in the three cluster shapes. The results are in agreement with the predication by Toulhouat and Kasztelan [76] using the Gibbs–Curie–Wulf law.

The diameter (D) of the regular hexagonal clusters can be described by a function of the number of the Mo_{IV} atoms in a $(30\bar{3}0)$ edge plane.

$$D = (2n - 1)a + 2R_S \quad (1)$$

where n is the number of the Mo_{IV} atoms in a $(30\bar{3}0)$ edge plane of the regular hexagonal clusters (Fig. 2); R_S is the atomic radius of S (the van der Waals radius of S being 1.7 Å); a is the crystal constant ($a = 3153$ Å). Assuming $2R_s \approx a$, then

$$D \approx 2na = 6.31n\,(\text{Å}) \quad (2)$$

The Mo_{IV}/Mo_{total} and S_{II}/S_{total} atomic ratios in the regular hexagonal clusters can be calculated by an equation that derived from the common formula of $Mo_{3n^2}S_{6n^2}$ (see Fig. 2) and Eq. (2):

$$Mo_{IV}/Mo_{total} = S_{II}/S_{total} = 1/n = 6.31/D \quad (3)$$

This equation indicates that the Mo_{IV}/Mo_{total} and S_{II}/S_{total} atomic ratios are equal and are the function of the size of the basal plane for the regular hexagonal clusters. This relationship should be very important and useful in the fundamental study of MoS_2 catalysts.

For the highly dispersed alumina-supported MoS_2 catalysts, the predominant size of MoS_2 particles is within 10–30 Å [28,43,44]. For the highly dispersed unsupported MoS_2 catalysts, the predominant size of crystal particles is within 40–130 Å [77]. If we consider the structure of highly dispersed MoS_2 particles in the size around 20 Å in combination with the stable peripheral structure, stoichiometry, and crystal shape as discussed above, the $Mo_{27}S_{54}$ cluster, as shown in Fig. 2, should be the best model for modeling highly dispersed MoS_2 particles. The peripheral edges of the $Mo_{27}S_{54}$ cluster consists of three $(\bar{1}010)$ edge planes and three $(30\bar{3}0)$ edge planes. Each $(30\bar{3}0)$ plane contains one $Mo_{IV}^{3,3,3,3}$ and two $Mo_{IV}^{2,2,3,3}$ atoms, while each $(\bar{1}010)$ plane contains two $S_{II}^{6,6}$ and four $S_{II}^{4,6}$ atoms. The average coordination number of Mo atoms in this model is 5.33, in good agreement

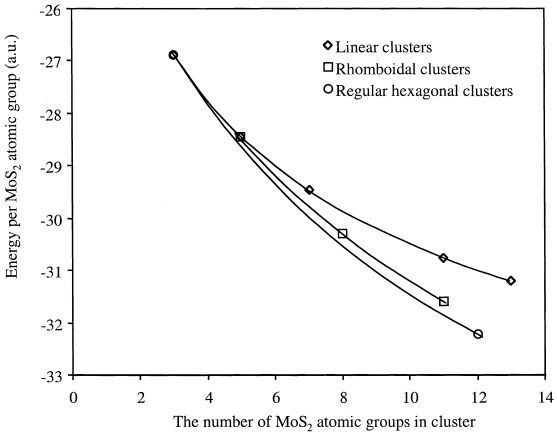

Fig. 3. Stability of clusters with different shapes.

with the experimental value (5.20 ± 0.5) obtained by EXAFS [50,51,66]. The atomic ratio of S_{II}/S_{total} in the cluster is 0.333. Interestingly, this S_{II}/S_{total} ratio in the $Mo_{27}S_{54}$ cluster is within the range of the S_{labile}/S_{total} ratios in a supported MoS_2 catalyst measured by ^{35}S-labeled HDS experiment [78], indicating that the S_{II} atoms in the cluster probably correspond to the labile S atoms in the surface of MoS_2 catalyst. It needs to be mentioned that in the sulfided atmosphere, e.g. in the presence of 5% H_2S in H_2, a weaker adsorption of H_2S at the coordinatively unsaturated Mo_{IV} atoms is possible at lower temperatures (< 200°C), leading to the excess or non-stoichiometric S atoms in the MoS_2 catalysts as observed in some experiments [68,77]. According to our MoS_2 model, these excess S atoms should be the S_I atoms in the $(10\bar{1}0)$ edge planes. However, at the HDS reaction conditions (200–400°C and lower H_2S partial pressure) since the experimentally measured S/Mo stoichiometry of supported and unsupported MoS_2 catalysts is around 2.0 or even slightly lower than 2.0 [68,77,78], the existence of S_I in the $(10\bar{1}0)$ planes of MoS_2 crystal is unlikely. The proposed $Mo_{27}S_{54}$ cluster in this study is similar to the model $Mo_{36}S_{72}$ predicted by Topsøe et al. [20] on the basis of their understanding. Their model is an approximate regular hexagonal cluster, in which two sulfur atoms in the $(\bar{1}010)$ edge plane are removed to maintain the Mo/S stoichiometry of the model.

3.1.3. Simplification of $Mo_{27}S_{54}$ cluster

As there is an atom-number limit in our calculation program, we designed a smaller, but still stoichiometric, $Mo_{16}S_{32}$ cluster, as shown in Fig. 4, to mimic the edge structure of the $Mo_{27}S_{54}$. Since the bottom plane $(\bar{1}010)$ and the top plane $(30\bar{3}0)$ in $Mo_{16}S_{32}$ cluster are respectively the same as the corresponding edge planes in the $Mo_{27}S_{54}$ cluster, we assume that the electronic properties of the edge planes calculated from the $Mo_{16}S_{32}$ cluster should be the same as, or very close to, those of the corresponding planes in the $Mo_{27}S_{54}$ cluster. The charge distribution and bond indexes of the $Mo_{16}S_{32}$ cluster were calculated and the results are listed in Tables 3 and 4, respectively. The coordinatively unsaturated Mo_{IV} in the $(30\bar{3}0)$ plane shows a positive charge, being $+0.291$

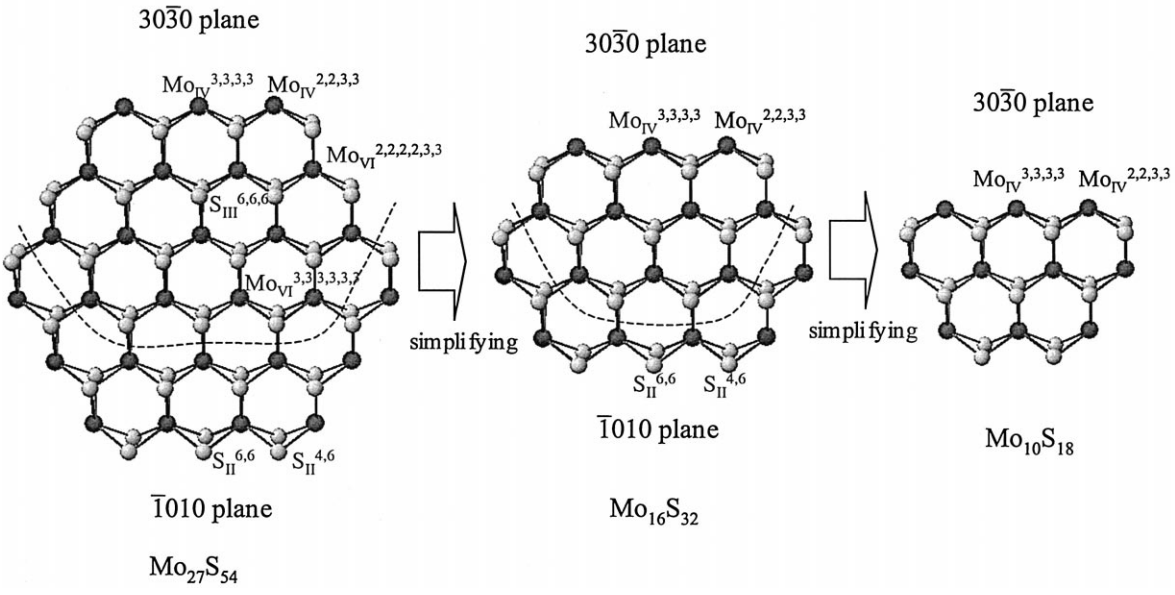

Fig. 4. Simplification of $Mo_{27}S_{54}$ cluster.

Table 3
Formal charge of the atoms in $Mo_{16}S_{32}$ cluster

Atom	Number	Average charge (a.u.)
$S_{II}^{4,6a}$	4	−0.261
$S_{II}^{6,6a}$	2	−0.212
$S_{III}^{4,4,6b}$	4	−0.129
$S_{III}^{6,6,6}$	10	−0.077
$Mo_{IV}^{2,2,3,3b}$	2	0.291
$Mo_{IV}^{3,3,3,3b}$	1	0.350
$Mo_{VI}^{2,2,2,2,3,3a}$	2	0.326
$Mo_{VI}^{3,3,3,3,3,3}$	5	0.248

[a] In the bottom edge plane of the $Mo_{16}S_{32}$ as shown in Fig. 3.
[b] In the top edge plane of the $Mo_{16}S_{32}$ as shown in Fig. 3.

and +0.350 (a.u.) for $Mo_{IV}^{2,2,3,3}$ and $Mo_{IV}^{3,3,3,3}$, respectively. The middle Mo_{IV} ($Mo_{IV}^{3,3,3,3}$) is more positive than the end Mo_{IV} ($Mo_{IV}^{2,2,3,3}$), indicating that the $Mo_{IV}^{3,3,3,3}$ is more ionizable. The bridge S atoms in the $(\bar{1}010)$ edge planes show a negative charge with a value of −0.261 and −0.212 (a.u.) for $S_{II}^{4,6}$ and $S_{II}^{6,6}$, respectively. The tribound S atoms in the basal planes have a lower negative charge, the average value being −0.077 (a.u.). The bond indexes for S_{II}–Mo and S_{III}–Mo are around 1.0 and 0.8, respectively, in agreement with those obtained from the $Mo_{12}S_{38}$ cluster. Since there is much evidence that the active sites for HDS involve CUS [20,50,51,65,66], we consider that the coordinately unsaturated Mo_{IV} in the $(30\bar{3}0)$ planes should have a significant role in HDS. In the following discussion, we will focus on the Mo_{IV} in the $(30\bar{3}0)$ plane.

In order to examine the interaction of sulfur species with the $(30\bar{3}0)$ edge plane, we designed another smaller cluster $Mo_{10}S_{18}$, as shown in Fig. 4, to mimic a $(30\bar{3}0)$ edge plane in consideration of the atomic number limit in our ZINDO program and of computational time. The $Mo_{10}S_{18}$ cluster has a $(30\bar{3}0)$ edge plane the same as that in the $Mo_{27}S_{54}$ cluster though it is not stoichiometric. We assume that the influence of the atoms at the positions far from the $(30\bar{3}0)$ edge plane on the properties of the $(30\bar{3}0)$ plane is negligible. The orbital populations (Mulliken) and formal charge of the $Mo_{IV}^{3,3,3,3}$ in the $(30\bar{3}0)$ plane of the $Mo_{10}S_{18}$ and $Mo_{16}S_{32}$ clusters were calculated. As listed in Table 5, the charge and orbital populations of the Mo_{IV} in the $(30\bar{3}0)$ plane of the $Mo_{10}S_{18}$ cluster is similar to those of the Mo_{IV} in the $(30\bar{3}0)$ plane of the $Mo_{16}S_{32}$ cluster. This indicates that the simplification of the $Mo_{27}S_{54}$ cluster by the $Mo_{10}S_{18}$ cluster is reasonable for examining the $(30\bar{3}0)$ plane.

Table 4
Bond indexes in $Mo_{16}S_{32}$ cluster

S–Mo	Bond index
$S_{II}^{4,6}$–$Mo_{IV}^{2,2,3,3}$	1.026
$S_{II}^{4,6}$–$Mo_{VI}^{2,2,2,2,3,3}$	1.018
$S_{II}^{6,6}$–$Mo_{VI}^{2,2,2,2,3,3}$	1.008
$S_{III}^{4,4,6}$–$Mo_{IV}^{2,2,3,3}$	0.806
$S_{III}^{4,4,6}$–$Mo_{IV}^{3,3,3,3}$	0.849
$S_{III}^{4,4,6}$–$Mo_{VI}^{3,3,3,3,3,3}$	0.776
$S_{III}^{6,6,6}$–$Mo_{VI}^{3,3,3,3,3,3}$	0.807

3.2. Interaction of the $(30\bar{3}0)$ plane with sulfur species

3.2.1. Adsorption configuration of thiophene on the $(30\bar{3}0)$ plane

In order to examine the interaction of the $Mo_{IV}^{3,3,3,3}$ with thiophene, we located the sulfur atom of thiophene at the S_I position in the $(10\bar{1}0)$ plane of the $Mo_{10}S_{18}$ cluster, and then

Table 5
Comparison of electronic properties of $Mo_{IV}^{3,3,3,3}$ between $Mo_{16}S_{32}$ and $Mo_{10}S_{18}$ clusters

	$Mo_{16}S_{32}$	$Mo_{10}S_{18}$
$Mo_{IV}^{3,3,3,3}$ charge (a.u.)	0.350	0.338
$S_{III}^{4,4,6}$–$Mo_{IV}^{3,3,3,3}$ bond index	0.849	0.856
Mulliken's orbital populations		
s	0.505	0.534
p_x	0.240	0.171
p_y	−0.113	−0.061
p_z	0.035	0.038
d_{z^2}	1.265	1.297
$d_{z^2-y^2}$	0.897	0.832
d_{xy}	1.122	1.149
d_{xz}	0.840	0.747
d_{yz}	0.331	0.421

changed the angle included between the molecular plane and the $(10\bar{1}0)$ plane, as shown in Fig. 5(T-θ). The total energies and pseudo-adsorption heat (ΔH) of thiophene–$Mo_{10}S_{18}$ at different angle were calculated. Other possible adsorption configurations where the S_T–Mo bond length of 2.415 Å is fixed, also shown in Fig. 5 and noted by A, B, C, D-0, D-45, D-90, and E, were also calculated. The results are listed in Table 6. The adsorption configuration (T-0) with the included angle of 0° was found to be the most stable one as the pseudo-adsorption heat ($\Delta H = -8.49$ (a.u.)) of thiophene–$Mo_{10}S_{18}$ for this configuration is the highest in absolute magnitude in all of the configurations. In other words, the adsorption configuration of thiophene parallel to the $(30\bar{3}0)$ plane, as shown in Fig. 6, is the most stable and the most probable one. Other adsorption configurations addressed in Fig. 5 are unlikely, as they have much lower pseudo-adsorption heats ($\Delta H \geq -6.75$ (a.u.)) in absolute magnitude than that for the flat adsorption configuration. From Fig. 6, it is also clear that thiophene is adsorbed on the Mo atom not only through a S_T–Mo bond, but also through bonds between π-electrons on the thiophenic ring and the Mo. The bond index values are 0.566, 0.507, 0.472, 0.473, and 0.507 for S_T–Mo, C_2–Mo, C_3–Mo, C_4–Mo, and C_5–Mo, respectively.

The calculated formal charge of the adsorbed thiophene for the flat adsorption configuration is $+0.872$ (a.u.), indicating that the electrons shift partially from the thiophene ring to the $(30\bar{3}0)$ plane during the adsorption process. In all of the adsorption configurations examined in this study, the formal charge of adsorbed thiophene for the flat adsorption configuration is the highest, which is in agreement with the highest pseudo-adsorption heat in absolute magnitude.

The calculated electrostatic potentials of thiophene and the $Mo_{10}S_{18}$ cluster are displayed in

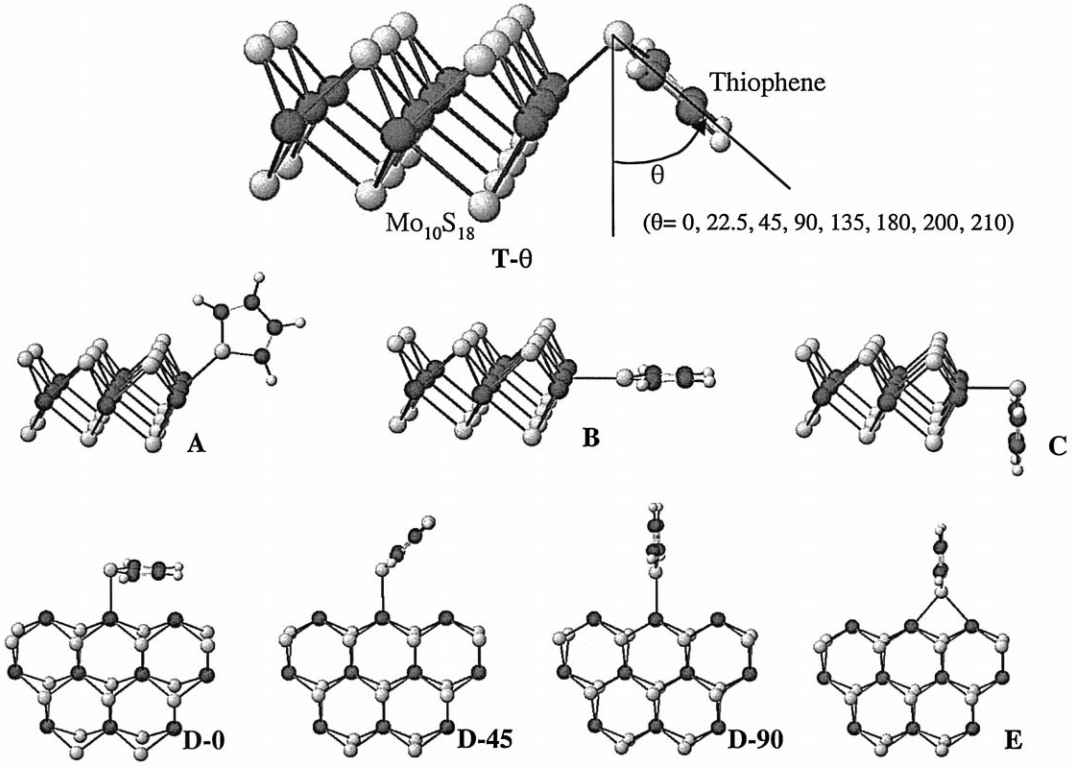

Fig. 5. Various adsorption configurations of thiophene on $Mo_{IV}^{3,3,3,3}$.

Table 6
Pseudo-adsorption heat and formal charge for different configurations

No. configuration	$Mo_{10}S_{18}$–thiophene			$Mo_{10}S_{18}$–THT		
	Total energy (a.u.)	ΔH (a.u.)	Charge of whole T (a.u.)	Total energy (a.u.)	ΔH (a.u.)	Charge of whole 4Ht (a.u.)
1. T-0	−333.93	−8.49	0.872			
2. T-22.5	−332.60	−7.16	0.869	×		
3. T-45	−331.66	−6.22	0.654	−335.81	−6.68	0.661
4. T-90	−330.88	−5.44	0.430	−335.08	−5.95	0.435
5. T-135	−330.77	−5.33	0.371	−335.06	−5.93	0.392
6. T-180	−331.25	−5.80	0.447	−335.84	−6.71	0.497
7. T-190				−336.21	−7.08	0.569
8. T-200	−331.80	−6.35	0.518	−336.78	−7.65	0.835
9. T-210	−332.14	−6.70	0.587	×		
10. T-220	×[a]					
11. A	−330.68	−5.23	0.551	−334.93	−5.80	0.375
12. B	−330.56	−5.11	0.424	−334.85	−5.72	0.454
13. C	−331.83	−6.38	0.663	−336.10	−6.97	0.681
14. D-0	−332.19	−6.75	0.804			
15. D-45	−330.87	−5.43	0.471			
16. D-90	−330.55	−5.11	0.423	−334.67	−5.54	0.416
17. E	−331.26	−5.82	0.618	−335.59	−6.46	0.642

[a]As the atoms between sulfur specie and MoS_2 cluster are too close, the SCF density calculation cannot be performed.

Fig. 7. The electron-rich regions around thiophene are located at two sides of the thiophene ring, whereas the $Mo_{10}S_{18}$ cluster shows a rich positive electrostatic potential on the $M_{IV}^{3,3,3,3}$ sites in the $(30\bar{3}0)$ plane in agreement with the charge distribution (see Table 3), indicating where the electron density is poor. It is clear that the electrostatic potentials are in favor of the flat adsorption configuration (T-0).

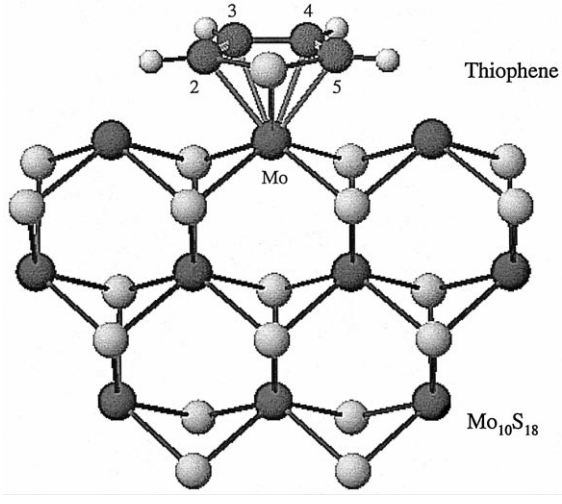

Fig. 6. The most stable adsorption configuration of thiophene on the $(30\bar{3}0)$ plane.

Molecular orbital calculations of the $Mo_{10}S_{18}$ cluster were also performed. The lowest unoccupied molecular orbital (LUMO) of the $Mo_{10}S_{18}$ cluster is shown in Fig. 8. The LUMO on the MoS_2 cluster is dominantly located on the $Mo_{IV}^{3,3,3,3}$ atom, indicating electron acceptor property of the $Mo_{IV}^{3,3,3,3}$ position. The results suggest that thiophene is most likely to donate the π-electrons to the $Mo_{IV}^{3,3,3,3}$. A significant increase in the total formal charge of thiophene and a decrease in the charge of the $Mo_{IV}^{3,3,3,3}$ were found during the flat adsorption process. The Mulliken's orbital populations also indicate that there might be a back donation of the electrons from the Mo to thiophene as the 5s and some 4d orbital populations of $Mo_{IV}^{3,3,3,3}$ decrease after the adsorption. However, the net electron transfer is from thiophene to the surface. The results, in good agreement with the electrostatic potential, support further the flat adsorption configuration.

From the coordination chemistry, a coordination geometry of thiophene with a transition

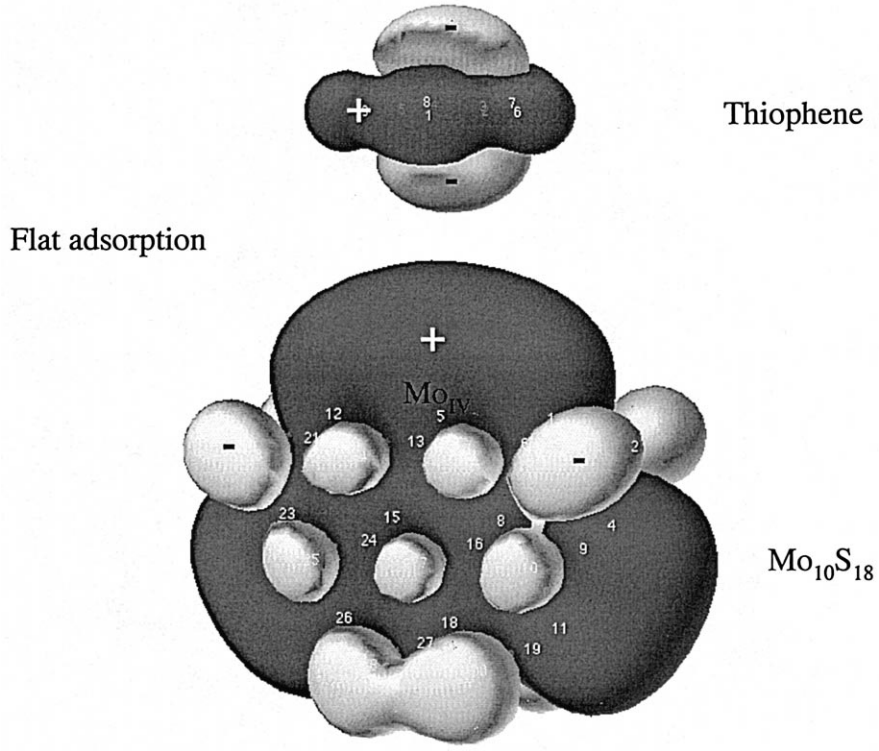

Fig. 7. The adsorption configuration suggested by electrostatic interaction.

metal through η^5-bonding has been reported to be one of the most common forms in transition metal complexes [79–89]. This η^5-bound geometry implies a probable form in the adsorption of thiophene on the surface, which is well consistent with the flat adsorption configuration derived from our molecular simulation.

The flat adsorption configuration obtained in this study is somewhat different from the flat adsorption configuration reported by Raybaus et al. [41], where thiophene coordinates with two Mo_{IV} atoms through a bridge–η^5 bonding. As Raybaud et al. used a periodic unit cell for modeling the $(30\bar{3}0)$ edge plane, the electron structure of each Mo_{IV} on the edge plane were equal. In our model, the electron structure at the middle Mo ($Mo_{IV}^{3,3,3,3}$) and the end Mo ($Mo_{IV}^{2,2,3,3}$) in the $(30\bar{3}0)$ plane are different as shown in Fig. 8 and Table 3. This may be a reason why the adsorption configuration obtained in this study is somewhat different from theirs, although both are the flat adsorption configurations. Another probable reason is no relaxation of the surface and the adsorbate in our work.

Analogous to thiophene, the flat adsorption configuration was found to be the most stable one for both DBT and naphthalene over the $(30\bar{3}0)$ plane, as shown in Fig. 9. The ΔH is -18.16 and -14.21 (a.u.), respectively. It was found that DBT and naphthalene interact with the $(30\bar{3}0)$ edge plane not only through a η^5-bonding or a η^6-bonding to the $Mo_{IV}^{3,3,3,3}$, but also through other bonds between aromatic C atoms in the adsorbate and other Mo_{IV} atoms because there are three exposed Mo_{IV} atoms in a same edge plane of the MoS_2 cluster. However, in the transition metal complexes there is only a mono-metal center or a bi-metal center at a special geometric space. This is a probable reason why such an adsorption configuration is

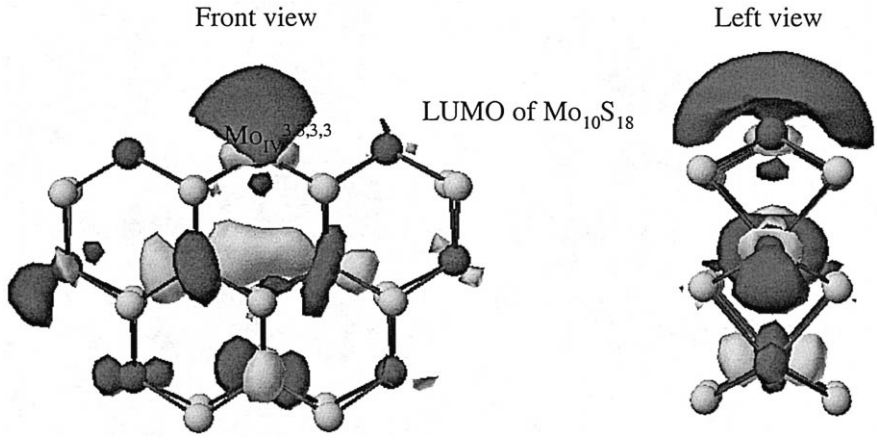

Fig. 8. The LUMO of $Mo_{10}S_{18}$.

not found in transition metal complexes of DBT. We believe that the flat adsorption configuration of thiophenic compounds and aromatics is responsible for the hydrogenation, and the Mo_{IV} in the $(30\bar{3}0)$ plane would be an active site for hydrogenation. Furthermore, since thiophenic compounds prefer the flat adsorption rather than a S-bound coordinative adsorption on the $(30\bar{3}0)$ edge plane, the direct hydrogenolysis of thiophenic compounds by the S-bound coordinative adsorption on the $(30\bar{3}0)$ edge plane would be unlikely.

3.2.2. Adsorption configuration of THT on the $(30\bar{3}0)$ plane

Some possible adsorption configurations of THT on the Mo in the $(30\bar{3}0)$ plane are shown in Fig. 10. The calculated total energies and electronic properties corresponding to various adsorption configurations are listed in Table 6. In all of the adsorption configurations addressed in this study, the tilted configuration (T-200), as shown in Fig. 11, where THT tilts to the $(10\bar{1}0)$ plane at an angle of 200°, was found to be the most stable one. The ΔH is -7.65 (a.u.), being

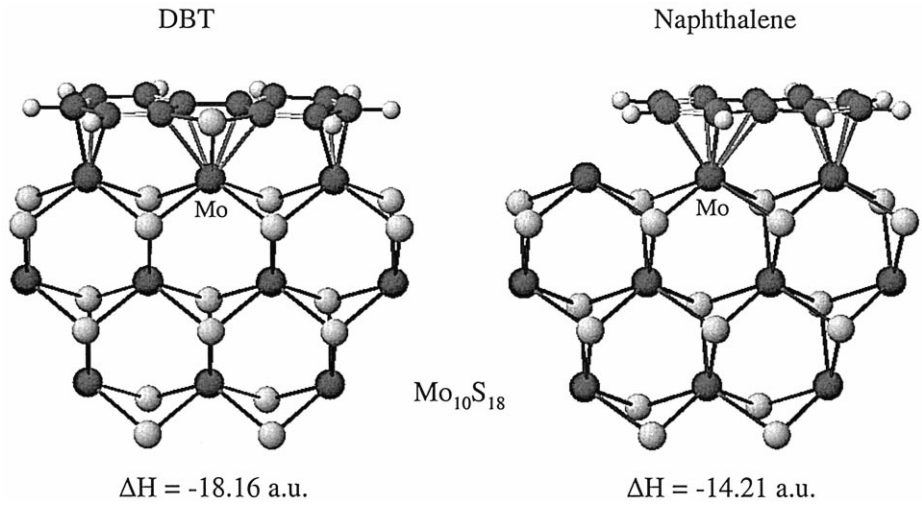

Fig. 9. The adsorption configurations of DBT and naphthalene on the $(30\bar{3}0)$ plane.

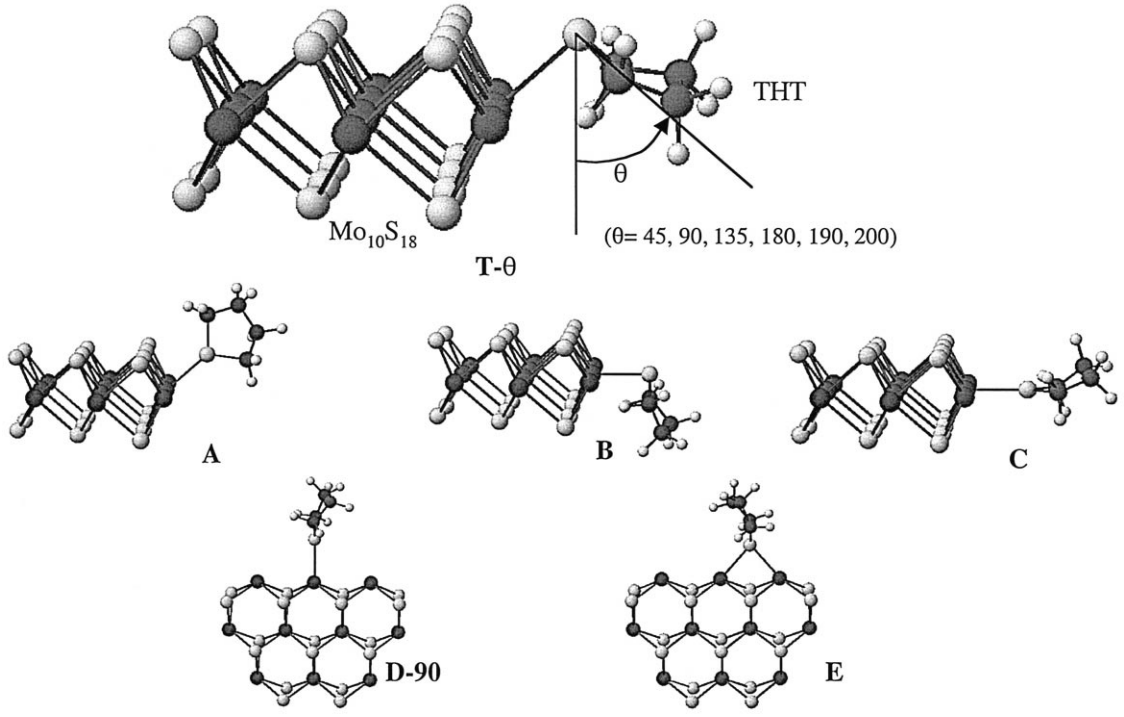

Fig. 10. Various adsorption configurations of THT on $Mo_{IV}^{3,3,3,3}$.

comparable to the ΔH (−8.49 a.u.) for the flat adsorption of thiophene. The Mulliken's orbital populations from our calculation indicate that there is a σ-bonding between the S_{THT} and the Mo where the S_{THT} might donate an alone pair to the Mo. The Mulliken's orbital populations also indicate a probable π-back donation from the Mo to the S_{THT} due to a decrease in some 4d orbital populations of the Mo. The net electron transfer is from the S_{THT} to the Mo. The

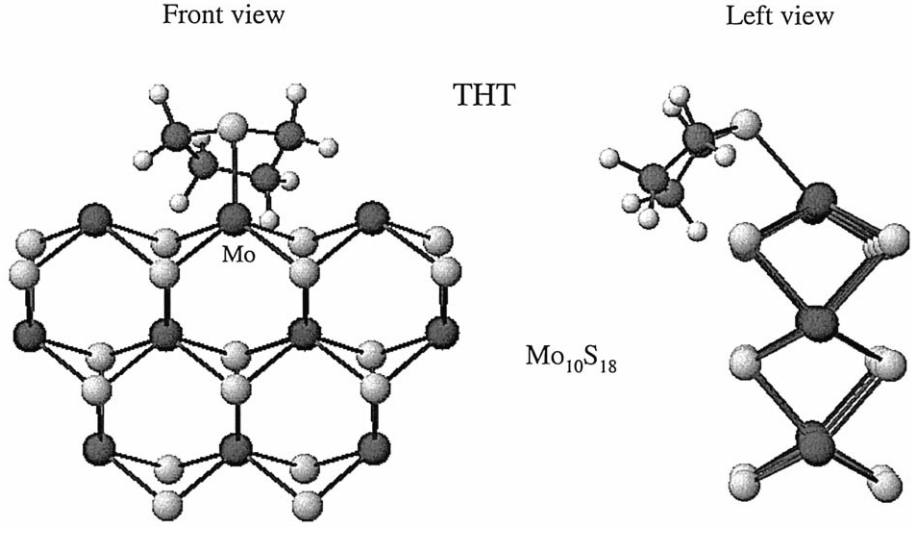

Fig. 11. The most stable adsorption configuration of THT on the $(30\bar{3}0)$ plane.

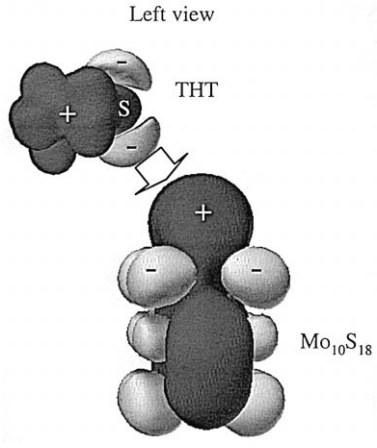

Fig. 12. The THT adsorption configuration suggested by electrostatic interaction.

electrostatic potentials of THT and the $(30\bar{3}0)$ plane, as shown in Fig. 12, strongly support the tilted adsorption configuration. According to the calculated ΔH and electrostatic potential analysis, other adsorption configurations of THT on the $(30\bar{3}0)$ plane are unlikely, although not necessarily impossible.

The higher negative electrostatic potential and the higher electron density concentrated on S_{THT} (electron density: 6.042) than those on S_T (electron density: 5.696) [90] indicate that S_{THT} is more readily subject to an electrophilic attack, in comparison with S_T, by a positive metal site at the catalyst surface, and more readily forms a S-bound coordinative adsorption. On the contrary, thiophene is more readily subject to an electrophilic attack in the direction perpendicular to thiophene plane. The tilted adsorption configuration of THT on the Mo also makes the C_2 and C_5 atoms of THT close to the surface of MoS_2, favoring an attack of the surface-activated hydrogen on the C_2 and C_5 atoms. Consequently, the S elimination from THT over the $(30\bar{3}0)$ plane might result from such tilted adsorption configuration of THT.

3.2.3. Adsorption of H_2S on the $(30\bar{3}0)$ plane

The adsorption configurations of H_2S on the $(30\bar{3}0)$ plane were also examined. Analogous to THT, a tilted adsorption configuration is the most stable. The corresponding ΔH value is -2.41 (a.u.), much lower in absolute magnitude than those for thiophene and THT. The lower ΔH value is favorable for the evolution of H_2S formed in HDS from the surface, and, thus, is favorable for the regeneration of the active side.

3.3. Hydrogenation pathway of thiophene on the $(30\bar{3}0)$ plane

The adsorption configurations of thiophene, THT, and H_2S on the Mo of the $(30\bar{3}0)$ plane in combination with the experimental observation from the literature [2,11,14,18] suggest a likely catalytic cycle procedure, as shown in Fig. 13, for the hydrogenation pathway of thiophene over MoS_2. Thiophene is first adsorbed on the Mo in the $(30\bar{3}0)$ plane by a η^5-bound coordination, and then hydrogenated to form an intermediate, THT. Because the ΔH of THT on the Mo by a S-bound coordination is close to that of thiophene by the flat adsorption, the formed THT might be likely adsorbed on the same Mo_{IV} and subsequently hydrogenolyzed to produce a hydrocarbon and a H_2S on the surface. The H_2S is then desorbed from the surface due to its weaker interaction with the Mo, and the active site is regenerated. Hence, we expect that the HDS of thiophene through the hydrogenation pathway would be likely to occur on the same active site (Mo_{IV}), but by the η^5- and S-bound coordinations for thiophene and THT, respectively. One may argue that desulfurization of thiophene and DBT by elimination of S atoms has been reported by many investigators in the literature [2–4,7,10,14,15,18,91–94]. We believe that such reactions would be likely to occur on the hydrogenolysis active sites rather than the hydrogenation active sites [7,45].

A much lower pseudo-adsorption heat of H_2S on the Mo, in absolute magnitude, than that of thiophene also implies that there would be no, or very weak, inhibition of H_2S against the hydrogenation of thiophene compounds, which

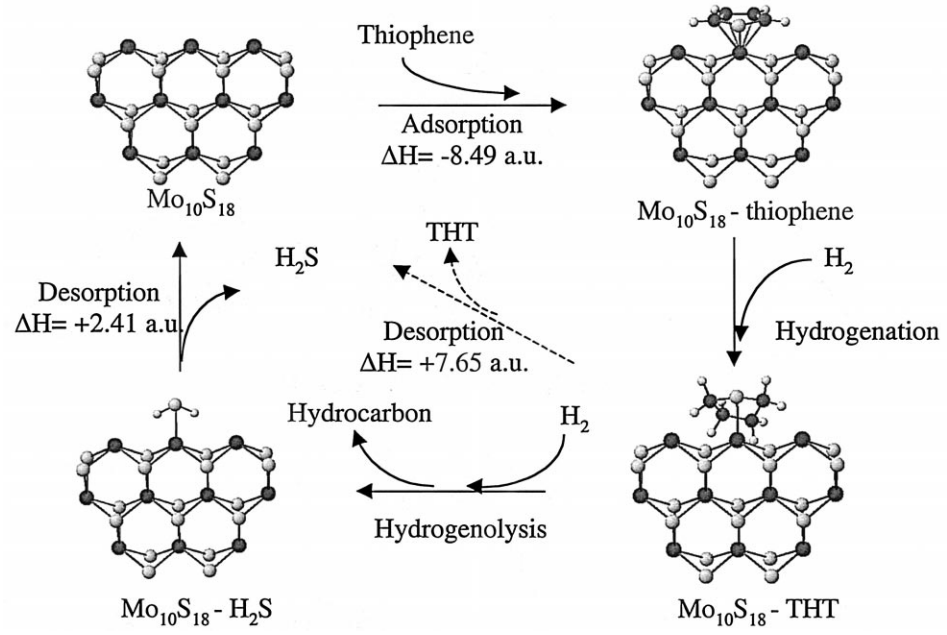

Fig. 13. HDS catalytic cycle of thiophene through hydrogenation pathway on the $(30\bar{3}0)$ plane.

coincides with the experimental results [9–15]. A higher pseudo-adsorption heat of naphthalene on the Mo_{IV} indicates that naphthalene probably inhibits the hydrogenation of thiophenic compounds strongly by a competitive adsorption on the same active site, which has been reported in previous experiments [15–17].

In this paper, we have addressed the active sites on the $(30\bar{3}0)$ plane of MoS_2 surface for hydrogenation of thiophenic and aromatic compounds, and also likely for the hydrogenolysis of THT, via the semi-empirical quantum chemical calculation. It should be emphasized that this work does not represent an exhaustive study, especially since we have not taken into account relaxation of the adsorbates. However, the reasonable agreement of our model and calculated results with many experimental results from the literature, as mentioned above, makes us believe that very useful results for HDS over MoS_2 can be obtained from the present approach. Many questions still remain. The location of the active sites on MoS_2 surface for the hydrogenolysis of thiophenic compounds and hydrogenated thiophenic compounds, as well as the hydrogenolysis pathway is not addressed in the present study. We are investigating this question [45], and the detailed results will be presented in a subsequent paper. The adsorption and dissociation of H_2 on the surface and the surface reaction of adsorbates are also very important issues for a fundamental understanding of HDS mechanism of thiophenic compounds. Further exploration is necessary to evaluate these issues.

4. Conclusions

In order to develop a fundamental understanding of the HDS mechanism of thiophenic compounds over MoS_2, a systematic molecular simulation of the HDS of thiophenic compounds over MoS_2 has been performed using ZINDO. On the basis of the calculated edge structure, stoichiometry of MoS_2, shape of the crystal, and the size corresponding to real MoS_2 particles, a single-slab cluster, $Mo_{27}S_{54}$, has been proposed for modeling the highly dispersed MoS_2 catalyst. The proposed cluster is a stoichiometric and regular hexagonal cluster with

$(\bar{1}010)$ and $(30\bar{3}0)$ edge planes only. The atomic ratio of S_{II}/S_{total} in the cluster is 0.33 and the average coordinative number of Mo atoms is 5.33, which is consistent with the previous experimental results in the literature. According to the calculated electronic properties on the surface, the coordinately unsaturated Mo_{IV} in the $(30\bar{3}0)$ plane is expected to be the active site for hydrogenation of thiophenic and aromatic compounds. The most stable configuration of thiophene on the Mo_{IV} is a flat adsorption configuration via the η^5-bound coordination, whereas the most stable configuration of THT on the Mo_{IV} is a tilted adsorption configuration via the S-bound coordination. HDS of thiophene through the hydrogenation pathway is likely to proceed on the Mo_{IV} sites in the $(30\bar{3}0)$ planes. An HDS mechanism of thiophene through the hydrogenation pathway has been proposed in the light of quantum chemical understanding, which is well in agreement with the experimental results from the literature.

References

[1] D.H. Killeffer, A. Linz, Molybdenum Compounds, Their Chemistry and Technology, Interscience, New York, 1952.
[2] J. Devanneaux, J. Maurin, J. Catal. 69 (1981) 202.
[3] M. Houalla, N.K. Nag, A.V. Sapre, D.H. Broderick, B.C. Gates, AIChE J. 24 (1978) 1015.
[4] C. Aubert, R. Durand, P. Geneste, C. Moreau, J. Catal. 97 (1986) 169.
[5] M.L. Virnat, Appl. Catal. 6 (1983) 137.
[6] A.V. Sapre, D.H. Broderick, D. Fraenkel, B.C. Gates, N.K. Nag, AIChE J. 26 (1980) 690.
[7] X. Ma, K. Sakanishi, T. Isoda, I. Mochida, in: M.L. Occelli, R. Chianelli (Eds.), Hydrotreating Technology for Pollution, Marcel Dekker, New York, 1996, p. 183.
[8] V. Vanrysselberghe, G. Froment, Ind. Eng. Chem. Res. 35 (1996) 3311.
[9] M. Nagai, T. Kabe, J. Catal. 81 (1983) 440.
[10] D.H. Broderick, B.C. Gates, AIChE J. 27 (1981) 663.
[11] I.A. van Panijs, G.F. Froment, Ind. Eng. Chem. Prod. Res. Dev. 25 (1986) 431.
[12] I.A. van Panijs, L.H. Hostenand, G.F. Froment, Ind. Eng. Chem. Prod. Res. Dev. 25 (1986) 437.
[13] T. Isoda, X. Ma, S. Nagao, I. Mochida, J. Jpn. Pet. Inst. 38 (1995) 25.
[14] J. Leglise, J.N.M. van Gestel, L. Finot, J.C. Duchet, J.L. Dubois, Catal. Today 45 (1998) 347.
[15] H. Farag, K. Sakanishi, I. Mochida, D.D. Whitehurst, Energy Fuels 13 (1999) 449.
[16] V. Lavopa, C.N. Satterfield, J. Catal. 110 (1988) 375.
[17] T. Isoda, X. Ma, I. Mochida, J. Jpn. Pet. Inst. 37 (1995) 506.
[18] J.M. Girgisand, C.B. Gates, Ind. Eng. Chem. Res. 30 (1991) 2021.
[19] D.D. Whitehurst, T. Isoda, I. Mochida, Adv. Catal. 42 (1998) 345.
[20] H. Topsøe, B.S. Clausen, F.E. Massoth, Hydrotreating Catalysis, Springer, Berlin, 1996.
[21] R.J. Angelici, Coord. Chem. Rev 105 (1990) 61.
[22] B.C. Wiegand, C.M. Friend, Chem. Rev. 92 (1992) 491.
[23] R.A. Sánchez-Delgado, J. Mol. Catal. 86 (1994) 287.
[24] R.J. Angelici, Bull. Soc. Chim. Belg. 104 (1995) 265.
[25] J.R. Dilworth, in: E.R. Braithwaite, J. Haber (Eds.), Molybdenum, Elsevier, Amsterdam, 1994, p. 477.
[26] W.D. Jones, D.A. Vicic, M. Chin, J.H. Roache, A.W. Myers, Polyhedron 16 (1997) 3115.
[27] C. Bianchini, A. Mell, Acc. Chem. Res 31 (1998) 109.
[28] A.N. Startsev, Catal. Rev. Sci. Eng. 37 (1995) 353.
[29] A.E. Gainza, E.N. Rodríguez-Arias, F. Ruette, J. Mol. Catal. 85 (1993) 345.
[30] R. Chen, Q. Xin, J. Mol. Catal. 64 (1991) 321.
[31] K. Teraishi, J. Mol. Catal. 126 (1997) 73.
[32] R. Pis Diez, A.H. Jubert, J. Mol. Catal. 73 (1992) 65.
[33] R. Pis Diez, A.H. Jubert, J. Mol. Catal. 83 (1993) 219.
[34] R. Chen, Q. Xin, C. Wang, J. Mol. Catal. 64 (1994) 345.
[35] R. Pis Diez, A.H. Jubert, J. Mol. Struct. 210 (1990) 329.
[36] M. Zonnevylle, R. Hoffmann, S. Harris, Surf. Sci. 199 (1988) 320.
[37] M. Daage, H.H. Murray, Prepr. Div. Petrol. Chem. ACS 38 (1993) 660.
[38] L.B. Byskov, B. Hammer, J.K. Norskov, B.S. Clausen, H. Topsøe, Catal. Lett. 47 (1997) 177.
[39] A. Tan, S. Harris, Inorg. Chem. 37 (1998) 2205.
[40] P. Raybaus, J. Hafner, G. Kresse, H. Toulhoat, Surf. Sci. 407 (1998) 237.
[41] P. Raybaus, J. Hafner, G. Kresse, H. Toulhoat, Phys. Rev. Lett. 80 (1998) 1481.
[42] X. Ma, H.H. Schobert, Prepr. Div. Fuel Chem. ACS 42 (1997) 48.
[43] F. Delannay, Appl. Catal. 161 (1985) 135.
[44] A.N. Startsev, V.I. Zaikovskii, Kinet. Katal. 35 (1994) 288.
[45] X. Ma, H.H. Schobert, Prepr. Div. Petrol. Chem. ACS 42 (1997) 657.
[46] P. Faye, E. Payen, D. Bougeard, J. Catal. 179 (1998) 560.
[47] R.W.G. Wyckoff, Crystal Structure, 2nd edn., Interscience, New York, 1963.
[48] J. Joffer, P. Geneste, D.A. Lerner, J. Catal. 97 (1986) 543.
[49] J.L.C. Daams, P. Villars, J.H.N. van Vucht, Atlas of Crystal Structure Types for Intermetallic Phases, ASM, Materials Park, 1991.
[50] S.M.A.M. Bouwens, D.C. Koningsberger, V.H.J. De Beer, S.P.A. Louwers, R. Prins, Catal. Lett. 5 (1990) 273.
[51] S.M.A.M. Bouwens, F.B.M. van Zon, M.P. van Dijk, A.M. van der Kraan, V.H.J. de Beer, J.A.R. van Veen, D.C. Koningsberger, J. Catal. 146 (1994) 375.
[52] M.C. Zerner, http://www.qtp.ufl.edu/zindo.html, Jan. 2000.

[53] J.A. Pople, D.L. Beveridge, Approximate Molecular Orbital Theory, McGraw-Hill, New York, 1970.
[54] J.A. Pople, D.L. Beveridge, P.A. Bobosh, J. Chem. Phys. 47 (1967) 2026.
[55] J. Ridley, M.C. Zerner, Theor. Chim. Acta (Berl.) 32 (1973) 111.
[56] J. Ridley, M.C. Zerner, Theor. Chim. Acta (Berl.) 42 (1976) 223.
[57] A.D. Bacon, M.C. Zerner, Theor. Chim. Acta (Berl.) 42 (1979) 21.
[58] M.C. Zerner, G.H. Loew, R.F. Kirchner, U.T. Mueller-Westerhoff, J. Am. Chem. Soc. 102 (1980) 589.
[59] W.P. Anderson, T.R. Cundarai, R.S. Drago, M.C. Zerner, Inorg. Chem. 29 (1990) 1.
[60] Molecular Simulation, http://www.msi.com/science/online/refreences/ZINDO References.html, Jan. 2000.
[61] J.J.P. Stewart, J. Comput. Chem. 10 (1989) 209.
[62] J.J.P. Stewart, J. Comput. Chem. 10 (1989) 221.
[63] G.A. Tsigdinos, Aspects of Molybdenum and Related Chemistry, Springer-Verlag, New York, 1978.
[64] S. Kassztelan, Langmuir 6 (1990) 590.
[65] R.J.H. Voorhoeve, J. Catal. 23 (1971) 236.
[66] S.M.A.M. Bouwens, J.A.R. van Veen, D.C. Koningsberger, V.H.J. de Beer, R. Prins, J. Phys. Chem. 95 (1991) 123.
[67] F.E. Massoth, J. Less-Common Met. 54 (1977) 343.
[68] F.E. Massoth, K.S. Chung, R. Ramachandran, Fuel Process. Technol. 2 (1979) 57.
[69] V.H.J. De Beer, C. Bevelander, T.H.M. van Sint Fiet, P.G.A.J. Werter, C.H. Amberg, J. Catal. 43 (1976) 68.
[70] A.N. Startsev, S.A. Shkuropat, E.N. Bogdanets, Kinet. Katal. 35 (1994) 282.
[71] W. Qian, A. Ishihara, S. Ogawa, T. Kabe, J. Phys. Chem. 98 (1994) 907.
[72] C. Calais, N. Matsubayashi, C. Geantet, Y. Yoshimura, H. Shimada, A. Nishijima, M. Lacroix, M. Breysse, J. Catal. 174 (1998) 130.
[73] G.A. Somorjai, Catal. Lett. 15 (1992) 25.
[74] E.I. Stiefel, Sci. Spectra 7 (1996) 62.
[75] M. Daage, R.R. Chianelli, J. Catal. 149 (1994) 414.
[76] H. Toulhouat, S. Kasztelan, in: J. Phillips, M. Ternan (Eds.), Proc. 9th International Congress on Catalysis, Calgary vol. 11988, paper No.152.
[77] C. Calais, N. Matsubayashi, C. Geantet, Y. Yoshimura, H. Shimada, A. Nishijima, M. Lacroix, M. Breysse, J. Catal. 174 (1998) 130.
[78] W. Qian, A. Ishihara, S. Ogawa, T. Kabe, J. Phys. Chem. 98 (1994) 907.
[79] A.E. Ogilvy, A.E. Skaugset, T.B. Rauchfuss, Organometallics 8 (1989) 2739.
[80] R.A. Sanchez-Delgado, R.L. Marquez-Silva, J. Puga, A. Tiripicchio, M. Camellini, J. Organomet. Chem. 316 (1986) C35.
[81] J.R. Lockemeyer, T.B. Rauchfuss, A.L. Rheingold, S.R. Wilson, J. Am. Chem. Soc. 111 (1989) 8828.
[82] E.A. Ganja, T.B. Rauchfuss, C.L. Stern, Organometallics 10 (1991) 270.
[83] S.C. Huckett, L.L. Miller, R.A. Jacobson, R.J. Angelici, Organometallics 7 (1988) 686.
[84] N.N. Sauer, R.J. Angelici, Organometallics 6 (1987) 1146.
[85] G.H. Spies, R.J. Angelici, Organometallics 6 (1987) 1897.
[86] J.W. Hachgenei, R.J. Angelici, Organometallics 8 (1989) 14.
[87] J.W. Hachgenei, R.J. Angelici, J. Organomet. Chem. 355 (1988) 359.
[88] S.C. Huckett, N.N. Sauer, R.J. Angelici, Organometallics 6 (1987) 591.
[89] D.A. Lesch, J.W. Richardson Jr., R.A. Jacobson, R.J. Angelici, J. Am. Chem. Soc. 106 (1984) 2901.
[90] X. Ma, K. Sakanishi, T. Isoda, I. Mochida, Energy Fuels 9 (1995) 33.
[91] G.H. Singhal, R.L. Espino, J.E. Sobel, G.A. Huff Jr., J. Catal. 67 (1981) 457.
[92] R. Edvinsson, S. Irandoust, Ind. Eng. Chem. Res. 32 (1993) 391.
[93] D.L. Sullivan, J.G. Ekerdt, J. Catal. 178 (1998) 226.
[94] Y. Iwata, K. Sato, T. Yoneda, Y. Miki, Y. Sugimoto, A. Nishijima, H. Shimada, Catal. Today 45 (1998) 353.